Mineralogia, vol. 52, 2021, 31-42 *Original paper*

DOI: 10.2478/mipo-2021-0004

New minerals and the first mineral occurrences in the Kupferschiefer (U, REE, HgS, chloride minerals $PtAs_2$, $Pt(Sb,Bi)_2$, $PtBi_2$), Poland, and their genetic meaning

Henryk "Harry" Kucha[1]†

[1] AGH University of Science and Technology, Faculty of Geology, Geophysics and Environmental Protection, al. A. Mickiewicza 30, 30-059 Kraków, Poland
†Corresponding author passed away on July 11, 2020

Abstract

Main U minerals in the Lubin and Polkowice mines in decreasing order of abundance are: uraninite, brannerite, metazunerite, metauranospinite, uranospinite, thucholite, monazite-huttonite, coffinite, and becquerelite. All these minerals are associated mainly with noble metal mineralization at the redox interfaces. Main minerals of REE are: (i) brannerite, monazite-huttonite in Noble Metals Bearing Shale (NMBS), (ii) florencite in Mo-Re shales and (iii) minor phospates in Cu-black shales derived from oxidation of organic matter. The latter, however, are controlling no more than 1/5 of the REE budget. Chloride minerals and sulphates are ubiquitous phases associated with Cu sulphides. They are represented by chlorargylite, cotunnite and penfieldite. Halite and sylvite form cubic inclusions in gypsum, up to 3 mm in chevrel compound, where they occur together with thiosulphates, annabergite and erithrite and Ni-Co-diarsenides. Sylvite is most common in lensoidal accumulations of semi massive kaolinite + chalcocite + gypsum at the contact between black shale and the top part of white sandstone. Such lenses have been traced over a distance of up to 30 m in the Lubin West and Polkowice East mines. Sylvite and halite have been so far overlooked during investigations of the Kupferschiefer because of applying standard cutting and polishing procedures using water as a lubricant. The Au content in native gold may reach exceptionally up to 97.40 wt% in a dolomitic reef from the Lubin West Mine. Gold forms four characteristic micro to nano-textures. Organic matrix of thucholite indicates correlation of Pt-Ni-V suggesting substitution of Pt in tetrapyrrole ring. Sperrylite, geversite and insizwaite appear at the western perimeter of Cu-sulphide deposit, where the redox gradient is so strong that almost all organic matter is gone. Platinum has forms its own minerals trapped in microfractures in anilite-digenite-spionkopite-yarrowite-bornite composite grains present in the reddened NMBS. Celestine-barite solid solution is one of the main accessory minerals in the Kupferschiefer. It has Sr/Ba ratio around 2.5 and 7.5. Euhedral uraninite associated with celestine-barite yielded U/Pb age of 84 ± 1 Ma, based on four grains measurements.

Keywords: Polish Cu deposits, phosphate, uranium, new occurrences of minerals

1. Introduction

This study is focused mainly on samples from active Polish Cu-mines: Lubin West, Polkowice East, Central and West and from the Sieroszowice Mine, where the major redox interface terminating copper ores occurs. All samples were collected at the contact between black shale and underlying sandstone and/or boundary dolomite stained red by epigenetic hematite, β-hydrohematite, akaganeite and goethite. Direct contact of organic matter rich shale with red sandstone has been used as a very well visible indicator of the redox interface (Rydzewski 1978; Kucha 1981; Kucha, Pochec 1983; Kucha et al. 1993) characterized by the highest redox gradient. The paper describes first occurrences of various minerals in this major Cu deposit and briefly discusses their genetic meaning.

2. Materials and Methods

Observations of fine noble metals and REE micro- and nano-textures were performed with a Hitachi S-4700 Field Emission Scanning Electron Microscope (FE-SEM) with cold cathode at the Institute of Geological Sciences, Jagiellonian University, Kraków, Poland.

Samples were cut and polished in a careful way avoiding water as a lubricant to prevent corrosion and dissolution of water soluble metal chlorides and compounds with mixed and intermediate S valences. Final polishing was done with a 1 µm diamond spray using light oil as a lubricant. This way a high-quality polishing surface was obtained allowing good resolution of fine micro-textures in polished sections with dry and oil objective lens of 50x and 100x magnifications. Nikon Eclipse LV100POL was used for observation of biogenic microtextures in reflected light at the Department of Applied Geosciences and Geophysics, Montanuniversität Leoben, Austria.

The chemical composition of minerals was determined with an ARL SEMQ electron microprobe and a Jeol JXA-8100-8200 microprobe at the Institute of Geological Sciences, Montanuniversität Leoben, Austria. Both microprobes were supplied with electronic system stabilizing beam intensity. Microprobe has been operated at 15/20 kV using the following standards and spectral lines: MgKα ($MgCO_3$), AlKα, SiKα, KKα ($KAlSi_3O_8$), Cl Kα (tugtupite), SKα and FeKα (FeS_2 cubic), CaKα ($CaCO_3$), MnKα, NiKα, ZnKα, AsLα, SeKα (PbSe), SbLα, SrLα (SrF_2), PdLα, AgLα, BaLα ($BaSO_4$), PtLα ($PtAs_2$), PbMα (PbS) and BiMα. To prevent sample decomposition under the beam all samples were cooled with liquid nitrogen.

Raman spectra were collected with a Dilor LABRAM confocal-Raman spectrometer equipped with a He-Ne laser (532 and 633 nm), and diffraction gratings of 1200 and 1800 grooves/mm. The registration of the spectra was accomplished with a Peltier-cooled, slow-scan CCD-matrix detector using 100x long distance working objective lens of an Olympus BX 40 microscope.

Reflectivity spectra were collected with a Zeiss microscope photometer MPM 400 using SiC and synthetic FeS_2 as standards.

Organic carbon was determined with a Leco elemental analyser at the Department of Applied Geosciences and Geophysics, Montanuniversität Leoben, Austria.

3. Uranium Minerals

3.1. Becquerelite $Ca(UO_2)_6O_4(OH)_6{\cdot}8H_2O$

Becquerelite occurs in coarse grained calcite replacing thucholite (Fig. 1a: A1, A2). It forms yellow-orange tabular crystals with pseudo hexagonal shape when viewed perpendicular to *001* (Fig. 1a: A1). When plates are oriented *010* perpendicular to the light, they obviously show needle-like orange intersections (Fig. 1a: A3), and color allows to distinguish them from dark brown brannerite needles (Fig. 1a: B1, B2). Becquerelite has size of up to 4 µm and yellow-orange or orange internal reflections.

The becquerelite contains from 1.95 to 2.25 wt% of Ca and from 0.85 to 1.30 wt% of Pb. This gives some excess of divalent cations in order of 0.1063 to 0.2204 pfu, respectively (Table A1), when compared to the ideal chemical formula of $Ca(UO_2)_6O_4(OH)_6{\cdot}8H_2O$.

The becquerelite studied by transmission electron microscopy (TEM) gives the following cell parameters: a = 13.536 ± 0.297, b = 12.298 ± 0.287, c = 14.313 ± 0.178, β = 90.50 ± 0.19°. The cell is monoclinic and systematic extinctions suggest monoclinic cell centered on bases (Fig. 1b,c). The β = 90.50 ± 0.19° can be directly measured from *010* diffraction pattern or calculated from pairs d values of 1 1 2 and 1 1 $\bar{2}$, 2 2 2 and 2 2 $\bar{2}$, 2 2 4 and 2 2 $\bar{4}$ etc. (Table A2). The correct quoted values of Miller indices can only be achieved for slightly modified unit cell with β = 90.50 ± 0.19° (Tables A3, A4, A5). Published earlier unit cell sizes measured by X-ray diffraction (XRD; Table A6; Piret-Meunier, Piret 1982; Pagoaga et al. 1987; Burns, Li 2002) have also been applied to registered electron diffraction patterns but a fit was less good then when the monoclinic unit cell has been used for calculations (Tables A3, A4, A5). The reason for the observed difference in crystal symmetry is not clear. The studied becquerelite contains Ca from 1.95 to 2.25 wt%, but unlike the formerly studied becquerelite it contains also from 0.85 to 1.30 wt% of Pb (Table A1). The presence of Pb causes some excess of divalent cations in order of 0.1063 to 0.2204 pfu (Table A1). It is not clear if such an excess could be sufficient to influence crystal symmetry and also to lower the c value from expected 14.920 down to the measured 14.313 by electron diffraction

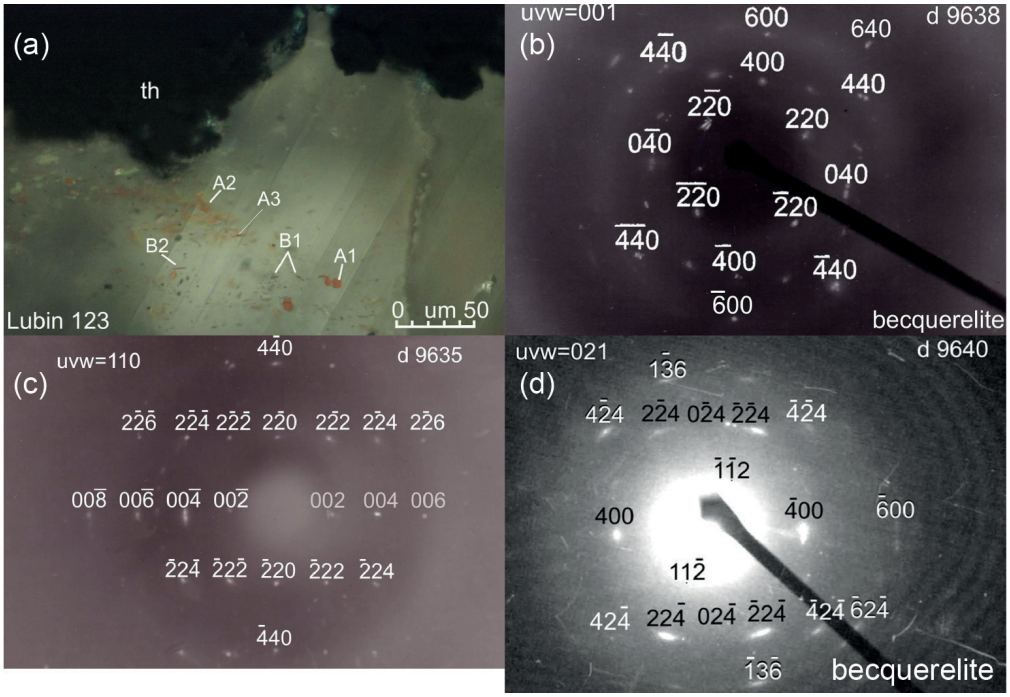

Figure 1. (a) Photomicrograph of tabular yellow to orange crystals of becquerelite (A1, A2, A3) and needles of brown to dark brown brannerite (B1, B2) embedded in the transparent matrix of twinned calcite (light) replacing thucholite (black, th). Note pseudo hexagonal outline of becquerelite plates. Reflected light, crossed polarizers. (b) The *001* electron diffraction pattern of becquerelite. Note that metamict decay causes some diffraction dots to split (2 2 $\bar{0}$, 4 4 0, 4 $\bar{4}$ 0, 4 4 0), or to occur as triple dots ($\bar{4}$ $\bar{4}$ 0, 0 $\bar{4}$ 0) although all nodes are sharp and well readable. (c) The *110* electron diffraction pattern of becquerelite. Note that metamict decay affects weakly only *00l* dots. (d) The *021* electron diffraction pattern of becquerelite. Note that an increasing curvature of the Ewald sphere for higher zone axes enhances visibility of the metamict distortion of diffraction nodes. Reflections 1 1 $\bar{2}$ and $\bar{1}$ $\bar{1}$ 2 probably occur by double diffraction.

(Table A6). The size of the pseudohexagonal platy fragments of becquerelite studied on TEM were small. The largest plate fragment measured was 150x120x25 nm. Such a small size of lattice fragments studied may probably reveal local fluctuations in the symmetry caused by metamict decay and/or Pb admixture.

Becquerelite is a secondary mineral created during oxidation of thucholite (Fig. 1a). The preliminary dating of this mineral shows two U/Pb ages of 134.9 and 88.9 Ma (Table A1).

3.2. Uraninite UO_2

Uraninite present in thucholite contains from 74.55 to 86.74 wt% of U (Table A1), and values range is similar to the range obtained by Banaś et al. (1978). The size of grains reaches up to 30 µm. Only one grain of uraninite was found with size of 2.8 mm and this grain was measured by Particle-induced X-ray Emission (PIXE) (Table A1; X1), the second grain had size 0.3 mm and was measured by µPIXE and Synchrotron X-ray Fluorescence Analysis (SXRFA) (Table A1: C14). Typical uraninite studied by TEM diffraction shows cubic symmetry with a = 0.542 ± 0.004 nm. Grains marked as altered (Table A7) are too small to be tested by XRD. Uraninite is subdivided into two groups by U/Pb ages (Table A1):

(i) 169 – 196 Ma (Table A1) comparable with age of homogenous A component of thucholite free of visible mineral inclusions measured by µPIXE and providing an age of 175 – 180 Ma (Kucha, Przybyłowicz 1999);
(ii) altered uraninite (Table A1) is occurring either on the edge of thucholite or is cut by microfractures seen on TEM. This uraninite type displays ages significantly younger and more variable, ranging from 58.8 to 161 Ma.

The Eu content seems to be higher in altered than in fresh uraninite (Table A1). Yttrium shows similar behavior (Table A1). Also the altered uraninite and its alteration products are enriched in Cu. Th and REE contents in uraninite are low (Table A1), only Ce, Nd and Sm contents are elevated. Uraninite occurs at the redox interface and contains slightly increased As, Fe and Cu (Table A1). Unfortunately overlaps between U and many of REE X-ray emission lines did not allow to detect and measure all of these elements in just 2 uraninite grains large enough for the PIXE beam size. Altered uraninite displays usually higher trace element admixtures than unaffected varieties of this mineral.

3.3. Brannerite $(U,Ca,REE)(Ti,Fe)_2O_6$

Brannerite present in the Kupferschiefer:

(i) occurs as inclusions in thucholite with size from 0.02 to 30 µm (Kucha 1993) (Fig. 2a-c), often associated with TiO_2 or sphene inclusions;
(ii) during oxidation of thucholite it forms brown to dark brown needles in replacive calcite matrix and it is associated with becquerelite (Fig. 1a);
(iii) in the matrix of the Noble Metals Bearing Shale (NMBS) it is present as subrounded grains with size of up to 50 µm. It forms characteristic microtextures composed from massive core built up from brannerite proper with reflectivity in air R% ~12, surrounded by a darker mineral with R% ~5 (Fig. 3a). The darker mineral may be either Si-bearing brannerite or U-bearing titanite. This mineral needs a further TEM study to clarify its mineral status, but due to a very small size of mineral particles and intergrowths this investigation will be challenging;
(iv) in the matrix of the NMBS occurs together with native gold, Pd-arsenides, Pd-arsenates, cobaltite-gersdorffite solid solution series, clay organic matter and grafene, covellite (cv), geerite (gr), spionkopite (sp), and organic matter (OM). It is tightly intergrown with muscovite-chloritised-illite intercalations and is surrounded by illite-organic matter matrix (Fig. 3b).

Analyses of brannerite from thucholite do not sum up to 100% (Table A8). The main missing element is C (and possibly N). The status of these elements needs a further study. The brannerite from thucholite, when compared to brannerite from the NMBS (Table A8), shows enrichment in Si, As, Fe, Cu, Al but contains less P, Y, Pr, Nd, Sm, Eu, Gd, and Zr (Table A8). One of the possible reasons may be serious age difference of both brannerite varieties in order of ~35 My as suggested by U/Pb dating (Table A8). Brannerite from thucholite is enriched in Cu (an average of 2.29 wt% of CuO) versus its counterpart from the NMBS (1.51 wt% of CuO on average, Table A8). Similar pattern is observed in the case of Fe and Al. The Zr content varies from 1.40 wt% average in thucholite, and around 1.99 wt% in brannerite from the NMBS (Table A8). This suggests that in organic carbon rich environment Zr is a mobile element. It is further confirmed by recuperation and overgrowths observed on detrital grains of zircon in the top part of white sandstone directly underlying the black shale.

Locally brannerite may be replaced by fine mixture of rutile and a darker mineral (R% in air ~15) tentatively identified as cleusonite $(Pb,Sr)(U^{4+},U^{6+})(Fe^{2+},Zn)_2(Ti,Fe^{2+},Fe^{3+})_{18}(O,OH)_3$, but more TEM and/or Raman data is required to confirm the identification of this phase.

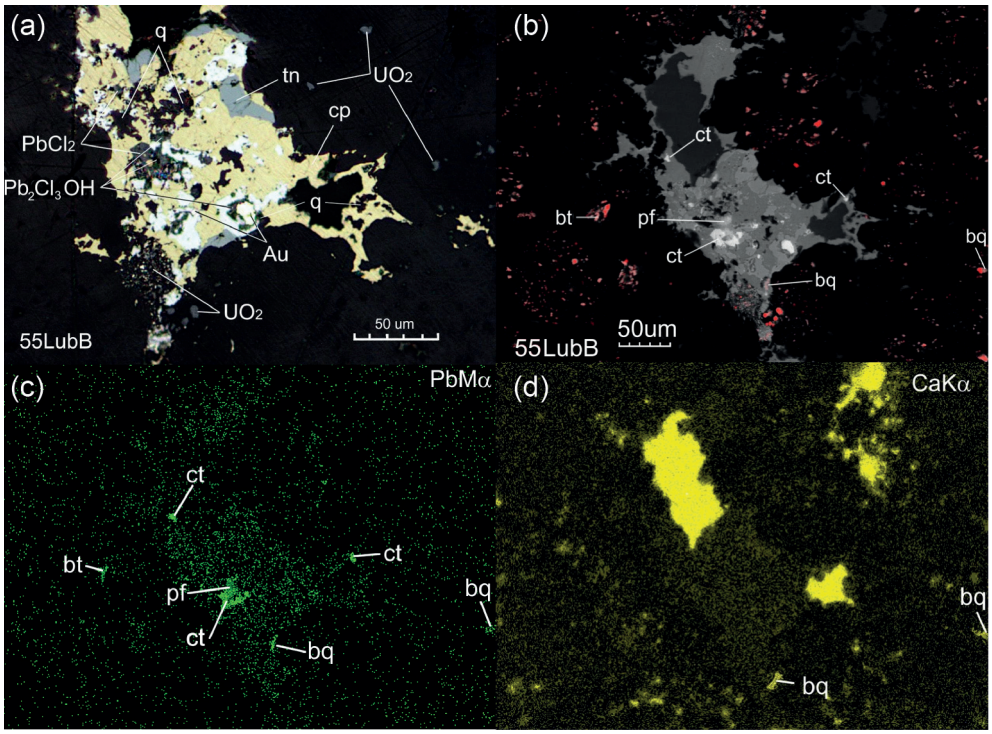

Figure 2. (a) Photomicrograph of complex noble metals assemblage: chalcopyrite (cp, yellow), cobaltite-gersdorffite (white), tennantite (tn, light grey), quartz (q) and calcite intergrown with gold (Au), cotunnite ($PbCl_2$), penfieldite (Pb_2Cl_3OH) and uraninite (UO_2), minor brannerite and Pb-bearing becquerelite. Black matrix is thucholite and minor calcite. Reflected light, sample 55LubB. (b) YAGBSE picture of mineral assemblage from Figure 2a showing in red U distribution: strong red isometric grains are uraninite, elongated medium/weak red are mainly brannerite (bt), medium red isometric are mainly becquerelite (bq) or coffinite. Penfieldite is marked as pf and is anhedral, cotunnite is marked as ct and is euhedral. (c) Distribution of Pb in the studied mineral assemblage. Cotunnite (ct, the highest Pb content), penfieldite (pf, medium Pb content), Pb-becquerelite (low Pb content, bq) and brannerite (bt) are marked. (d) Distribution of Ca in the studied mineral assemblage. Large grains represent calcite infillings with yellow-orange internal reflections, small grains appear as progressing replacements of thucholite by calcite advances, bq denotes becquerelite with some Pb content (see Table A1).

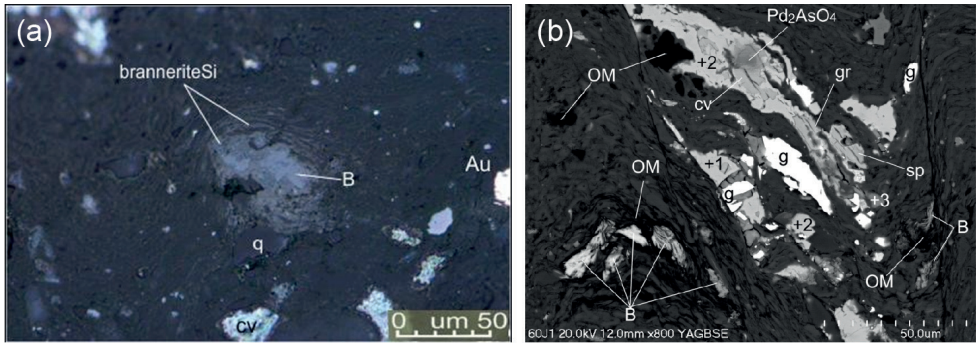

Figure 3. (a) Brannerite (B) in the matrix of the Noble Metals Bearing Shale (NMBS). Note that the shale lamination is swelling around brannerite suggesting its growth after deposition of the shale. q - quartz, branneriteSi - silica enriched brannerite. The micro texture of zoned brannerite-Si (or U-bearing titanite) suggests that it has been formed during replacement of the shale matrix. Au - gold, cv - covellite. Reflected light, sample Lubin West 60. (b) YAGBSE picture of two micro textural types of brannerite (B) in the NMBS: one semi massive and another intercalated with clay organic matter and graphene. Other minerals are native gold (g), cobaltite-gersdorffite(+1q), Pd_2As (+2, +3), Pd_2AsO_4, covellite (cv), geerite (gr), spionkopite (sp), organic matter (OM), muscovite-chloritised-illite and illite-OM matrix. Sample Polkowice East (PW27).

Brannerite appears to be the most durable U mineral in the studied Kupferschiefer samples. It has been found in the NMBS in Lubin West, Polkowice East, Polkowice Central, Polkowice West and Sieroszowice mines as one of the major accessory minerals accompanying Au and PGM’s (Kucha 1974; 1981; 1982; 1993).

3.4. Coffinite $U(SiO_4)_{1-x}(OH)_{4x}$ and monazite-huttonite

Coffinite was first described in the Kupferschiefer (Salamon, Banaś 2002) in the top part of the white sandstone. The area of its occurrence is extending from the Lubin West, through Polkowice East and Central to Sieroszowice East mines. It occurs in paragenetic assemblages containing red/brownish stains, thucholite, castaingite cobaltite-gersdoffite solid solution, nickeline, maucherite and rammelsbergite. Coffinite forms botryoidal rims on and replacements of detrital quartz grains. The associated Cu content in bulk samples is low and equals to 0.18 - 0.67 wt%.

Coffinite studied here occurs together with monazite-huttonite, castaingite and pyrite. These minerals are enclosed in euhedral quartz (Fig. 4a-c), where they are protected from later exchange of elements with surrounding matrix and fluids. Coffinite forms small botryoidal finely zoned spheres with size up to 6 - 8 µm. Surprisingly, coffinite shows from 4.23 to 5.91 wt% of MoO_2 (Table A9). Both coffinite and monazite-huttonite show some shortage of cations versus anions pfu. This may be connected with some still undetected cations. Further investigations by TEM and Raman are needed. Monazite-huttonite is older than coffinite by about 40 Ma (Table A9). More Th-U-Pb dating is needed to confirm the age measurements and to discuss their significance.

3.5. Metazunerite $Cu(UO_2)_2(AsO_4)_2{\cdot}8(H_2O)$, metauranospinite $Ca(UO_2)_2(AsO_4)_2{\cdot}8(H_2O)$ and uranospinite $Ca(UO_2)_2(AsO_4)_2{\cdot}10(H_2O)$

Metazunerite-metauranospinite and uranospinite are marker minerals of the major redox interface crossing the Kupferschiefer at Sieroszowice/Polkowice Mine at the border with a large Rote Fäule area. They are associated with Au-Ag solid solution, teterauricupride, tennantite, sulfo-arsenides of Co, Ni and Cu, di-arsenides of Ni and Co and nickeline, hematite, goethite ± akaganeite, and locally with cinnabar (Fig. 4b,c), $PtAs_2$, $Pt(Sb,Bi)_2$ and $PtBi_2$ (sperrylite group minerals, Figs 5, 6). Metazunerite, metauranospinite and uranospinite have reflectivity in air in order of 8-10%, and against bright ore minerals are poorly resolved in reflected light (Fig. 4b). However, in BSE images due to high average Z number they are very well visible (Fig. 4c), and clear-cut micro-zonation is revealed within banded metazunerite-metauranospinite. Uranospinite forms separate overgrowths on Ni-Co-arsenides (Fig. 4a-c). Some grain aggregates discussed are up to 0.5 mm and therefore they are visible even by naked eye in polished sections (Fig. 4a).

Metazunerite and metauranospinite form fine overgrowths of fractures and earlier mineral grains resembling oscillatory zoning with zone thickness from 0.1 to 2 µm (Fig. 4c). They have composite chemistry. Main elements are U, Zr, Cu and Ca as main cations (Table A10). Main anion is arsenate with significant substitution by SiO_4, PO_4 and less TiO_4 and H_2O is close to 8 pfu (Table A10). Main REE are La and Ce but they stay below 0.20 wt%.

Uranospinite forms separate overgrowths (Fig. 4c) and differs in number of main anions: SiO_4, PO_4, AsO_4 and less TiO_4 and H_2O are close to 10 pfu (Table A11). It contains less Zr, almost no Cu and Ca as the main cations

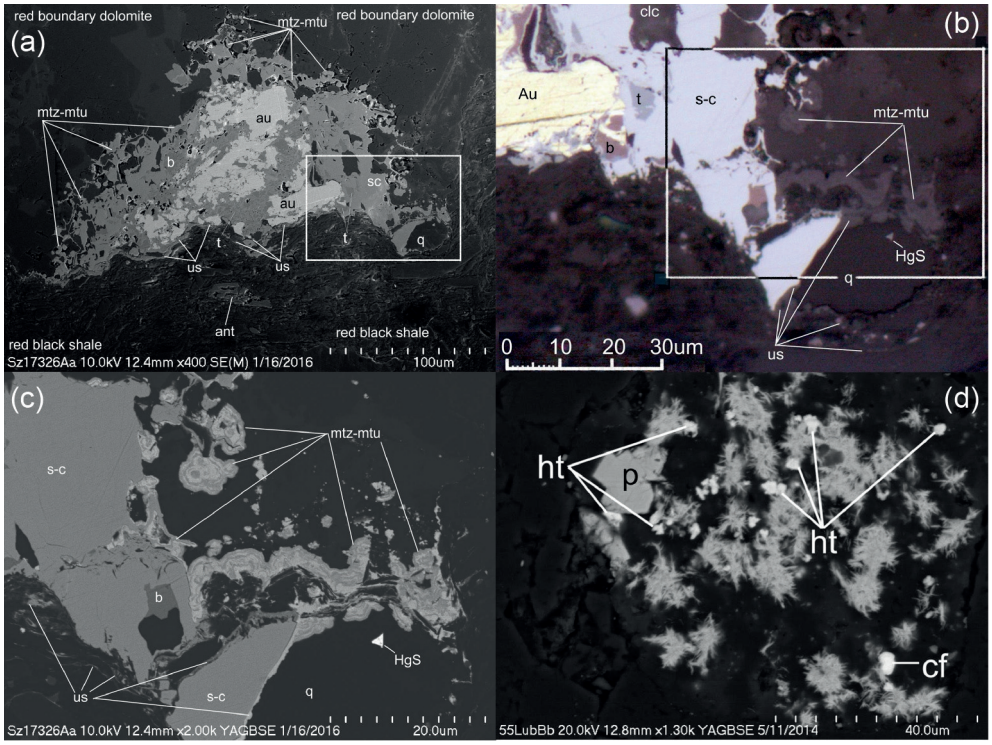

Figure 4. (a) SEM picture of gold (light grey, au) surrounded by mixed matrix composed of safflorite and clinosafflorite (grey, s-c), tennantite (darker grey, t), bornite (b) and uranium minerals metazunerite-metauranospinite (mtz-mtu ss), uranospinite (us), anatase (ant), quartz (q) and hematite ± akaganeite. Mineral composite grain is located exactly on the boundary between the reddened black shale and red boundary dolomite. Boxed area is magnified on Fig. 4b. Sample Sz1732 Sieroszowice Mine. (b) Photomicrograph showing ore mineralization composed from safflorite and clinosafflorite and gold (Au) intergrown and surrounded by banded metazunerite-metauranospinite, uranospinite, bornite, quartz and cinnabar. Boxed area shown on BSE picture on Fig. 4c; reflected light. (c) YAGBSE picture showing finely banded metazunerite-metauranispinite, uranopspinite and intergrown safflorite-clinosafflorite, and cinnabar encapsulated in overgrown quartz. (d) YAGBSE picture of euhedral quartz matrix containing radiating clots of castaingite needle crystals (light grey), euhedral huttonite-monazite (ht), finely zoned coffinite (cf), and euhedral pyrite (p). Sample 55, Lubin West Mine.

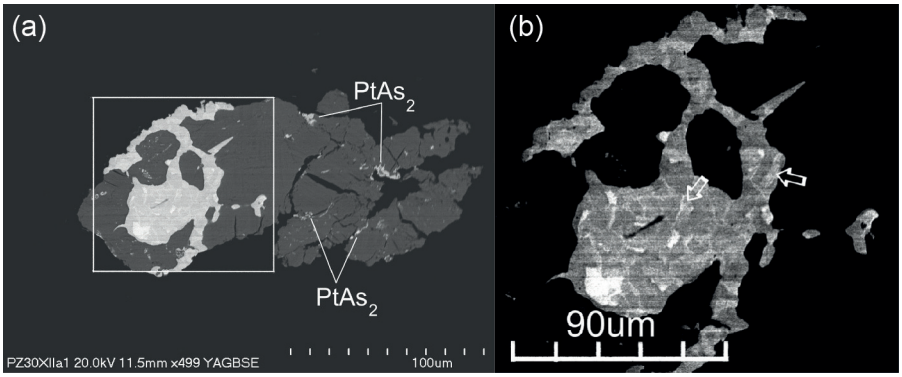

Figure 5. (a) YAGBSE picture of complex gold grain and sperrylite ($PtAs_2$) occurring in microfractures. Black matrix is anilite, spionkopite, digenite and covellite. Sample PZ32, Polkowice West Mine. Boxed area is shown on Fig. 5b. (b) YAGBSE picture of complex gold grain with local traces of oscillatory zoning (arrowed) due to change of Cu-Ag-Au proportions (wt%): Cu = 0.34 to 18.93, Ag = 15.32 to 74.86, Au = 16.99 to 84.65, Hg ≤ 0.08 to 9.01. Black matrix is anilite, digenite and spionkopite.

(Table A11), which clearly distinguishes this mineral from metazunerite/metauranospinite.

3.6. Florencite $(La,Ce,Nd,Sr)(Al_3Fe^{3+})(PO_4,SiO_4,SO_4)_2(OH)_6$

Florencite is a characteristic marker mineral connected with Mo-Re-rich shales occurring in the Western Lubin Mine, Eastern Polkowice Mine and Southern and Central Rudna Mine. It forms grains with size from a few to 20 μm and often it is intergrown by castaingite ($CuMo_2S_5$). It has a complex chemical composition (Table A7). Main anion is PO_4, but it can be substituted by up to 3.5 wt% of SO_4 and SiO_4. Main cation is Al. REE are represented by Ce, La, Nd, Pr, and smaller amount of Sm and Gd (Table A7). The SrO content varies from 1.66 to

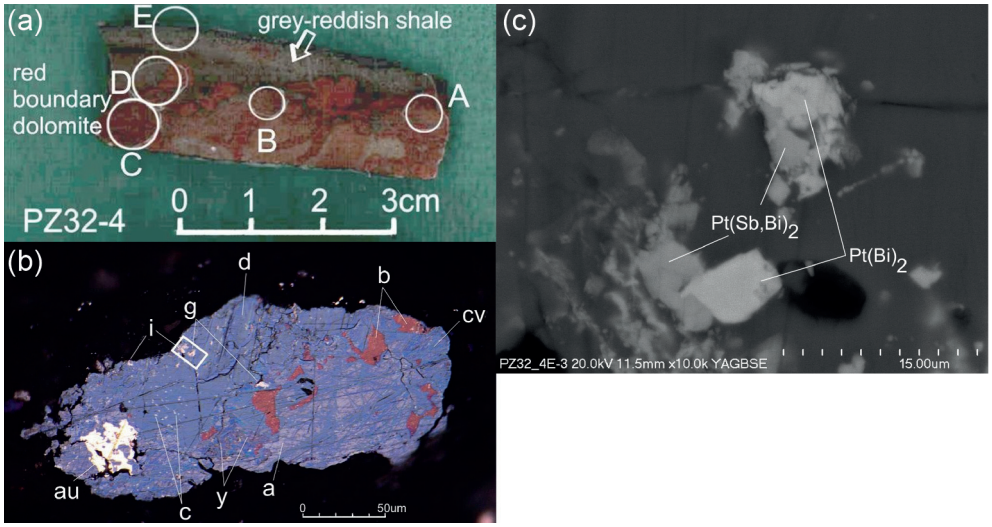

Figure 6. (a) Photomacrograph of grey-reddish Noble Metals Bearing Shale (NMBS) and red boundary dolomite marking redox interface in the Polkowice-Sieroszowice Mine. All Fe in carbonates and silicates (clays) is Fe^{3+}, almost all organic matter is oxidized and Pt has no place to hide and forms sperrylite, geversite and insizwaite in grey reddish shale (E). (b) Photomicrograph of composite grain of anilite (a), digenite (d), yarrowite (y), covellite (cv) and bornite (b) containing inclusions of gold (au), geversite (g), insizwaite (i), clausthalite (c). Cu-sulphide matrix is cut by fine twisted microfractures which are guiding later insizwaite and geversite. Black matrix is a few mm thick reddened NMBS. Reflected light, oil, sample PZ32-4E. Boxed area magnified on Fig. 6c. (c) BSE picture of insizwaite PtB_2 and geversite $Pt(Sb,Bi)_2$ in the dark grey matrix of anilite, digenite (d), yarrowite (y), covellite (cv).

5.93 wt%. Uranium is present in trace amounts and lack of Y may suggest that components needed to form florencite have been brought up by fluids containing very little of this element. Ca, Fe, K and Na form admixture at a level of 0.X to 1.5, exceptionally 3.7 wt% in case of K_2O (Table A7). Florencite is a main REE mineral in Mo-Re shales. Sample of Mo-Re rich shale dated by Re-Os isotopes shows age of 162.3 ± 0.8 Ma (Alderton et al. 2016).

3.7. Other phosphates

Calcium phosphates are common minerals in black shales and bioclastic reefs developed locally instead of black shales (Kucha, Pochec 1983). The P_2O_5 content in typical Cu black shale varies from 0.07 to 0.16 wt% (270 channel samples, KGHM), in Zn-bearing shale 0.09 - 0.88 wt%, in the NMBS 0.91 - 1.60 wt%. In the NMBS white phosphate lenses are intergrown with β-boracite (Kucha 1982; 1983).

The phosphate content may reach locally 1.0 - 1.5 wt% in bioclastic dolomitic reefs with native alloys of Au, Pt, Pd and Pb alloys with phosphates, red stains of β-hydrohematite and a few mm large glauconite grains. The REE content in these reddish phosphates is below 1 wt%.

The size of early diagenetic, banded phosphate lenses present in black shale varies from a few dozen µm up to a few cm in length (Kucha 1982; 1983). The REE content does not exceed 0.1 wt%. The source of P for these phosphates is decaying organic matter during early diagenesis.

Red Ca-phosphate lenses are up to 7 cm long and 1 cm thick. They are composed mainly from P, Ca, Fe, and F. REE, U, and Cu are present at a maximum level of a few tenths of wt%. The red lenses contain native gold, akaganeite and less hematite, β-hydrohematite and goethite.

There is yet another type of Ca-phosphates which are euhedral, small, and granular. They form grains from a few to 40 µm in size. A source of P for these phosphates may be evolving organic matter at late diagenetic stages. However, taking into account different heavy element signatures and contents, metal laden fluids circulating through the basement rocks (Blundell et al. 2003) at later stages of mineralization (Alderton et al. 2016) are more viable. These phosphates are Ca-phosphates with REE and Sr content not exceeding a few tenths of wt%. Similar content range applies to Si, Ti and S substituted for P.

4. Metal Chlorides

4.1. Cotunnite $PbCl_2$ and penfieldite $Pb_2Cl_3(OH)$

Cotunnite and penfieldite occur as accessory minerals in the NMBS and the Boundary Dolomite in the Lubin West and Polkowice East mines and their occurrence extends towards the Rudna Mine. They are present in mineral assemblage consisting of chalcopyrite, cobaltite-gersdorffite ss series, tennantite, native gold, uraninite, brannerite, becquerelite and quartz (Fig. 2). It is likely that Pb in assemblages connected with U minerals may be of radioactive provenance. Lead chlorides may be present also locally in the top part of white sandstone

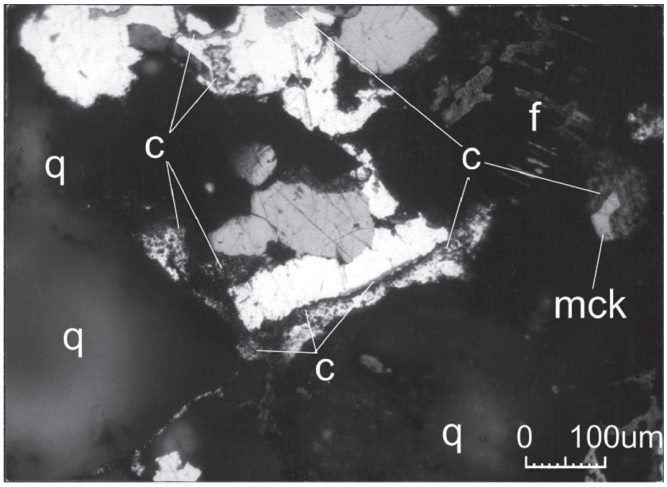

Figure 7. Photomicrograph of complex intergrowths of galena (light grey), Ag-amalgams (white), chlorargyrite (c), mckinstryite (mck) replacing feldspars (f) and filling up inter particle porosity between quartz (q) grains. Note that chlorargyrite shows minute replacing inclusion of Ag-amalgams shining white through transparent encompassing chlorargyrite. Sample 120T, reflected light.

together with chalcocite and galena and replacive yarrovite and castaingite.

Cotunnite and penfieldite form grains of up to 30 - 35 µm in size. The first mineral appears euhedral, the second either replaces the first or replaces galena alongside the edges. Cotunnite has reflectivity in air about 13%, and penfieldite about 9% in air. Cotunnite contains small admixture of S, Fe and Cu (Table A12).

So far cotunnite and penfieldite were found only as products of oxidation of thucholite or as products of replacement of chalcocite + galena in the top part of white sandstone directly below the Cu-bearing horizon, where locally Pb and Ag enriched sub-horizon occurs containing 0.25 m thick black shale with 1.40 wt% Cu, 5.82 wt% Pb, 109 ppm Ag and 1.60 m thick white sandstone with 0.32 wt% Cu, 0.64 wt% Pb and 50 ppm Ag (Kucha, Głuszek 1983).

4.2. Chlorargyrite AgCl

Silver chloride was first described in the Kupferschiefer in the top part of white sandstone, where the edges of Cu and Pb horizons overlap (Kucha, Gluszek 1983; Kucha 1990; vertical channel sample profile Ko7/27). The Pb horizon descends down to the white sandstone top, and such a mixed Cu/Pb layer, 0.5 to 1 m thick, extends down to the central part of the Rudna Mine as a belt ca 4 km long from the central part of the Lubin Mine to the central part of the Rudna Mine. The metal content in this horizon changes between (wt%): Cu = 0.40 - 1.29 (av 1.05), Pb = 1.81 - 9.92 (av 3.83), Zn = 0.62 - 3.11 (av 1.04), and (ppm): Ag = 1500 (av 236), Hg = 9 - 800 (av 61) (Kucha 1990).

The Cl content varies from 0.04 to 0.63 wt% and is associated with the presence of KCl (Kucha, 1990), NaCl, substitutions of Cl in Ca-sulphates and with chloragirite (Fig. 7, Table A13). Chlorargylite is replaced by silver amalgams (Fig. 7, Table A14).

4.3. Sylvite plus gypsum

There are two paragenetic assemblages where potassium chlorides occurs together with Cu and/or Mo sulphide mineralization:

(i) the most common is connected with lensoidal accumulations of semi massive kaolinite + chalcocite + gypsum + sylvite at the contact between black shale and the top part of white sandstone. Such lenses have been traced over a distance of up to 30 m in the Lubin West and Polkowice East mines. The main minerals constituting these lenses are kaolinite with thickness up to 4 cm and chalcocite containing myriads of small inclusions of gypsum, minute cubes of sylvite, euhedral quartz, ankerite, Mn-dolomite, and calcite (Fig. 8). Kaolinite forms booklets inside chalcocite or massive accumulations of crystals attaining size of up to a few mm. Kaolinite contains from (wt%) ≤ 0.01 to 1.85 Cu. Monazite present in the ore assemblage contains (wt%): Th = 4.10 - 6.14, U ≤ 0.09 - 1.23 and Ce, La, Nd and Sm as main REE. This is characteristic hyper saline assemblage marked by unusually high Th content in monazite. Such mineral assemblages are relatively common, but to notice them samples have to be cut and polished without water as a lubricant, otherwise water soluble small crystals of gypsum and sylvite will be dissolved and

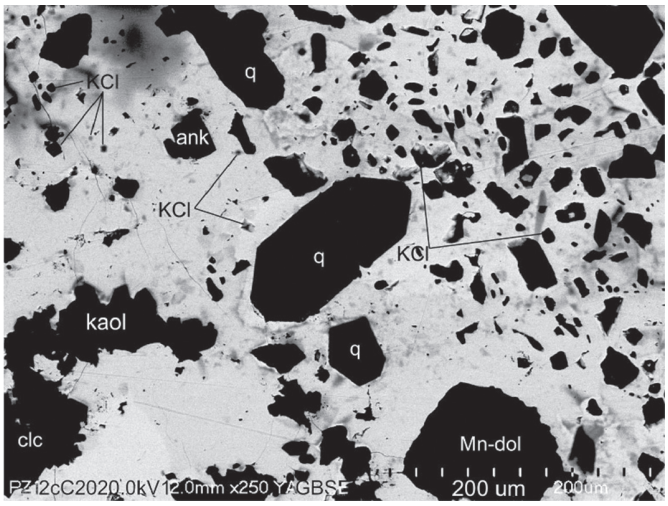

Figure 8. YAGBSE picture of massive chalcocite (white) full of inclusions of euhedral quartz (q), ankerite (ank), Mn-dolomite (Mn-dol), calcite (clc) and numerous sylvite grains with cubic outline (KCl). Black unstated inclusions are myriads of gypsum grains. Chalcocite is embedded into kaolinite discontinuous lens about 20 m long and 0.5 to 4 cm thick located directly between the black shale and the white sandstone top. Sample PZ12cC20.

will go unnoticed. A co-occurrence of myriads of gypsum inclusion pared by the presence of sylvite cubes (Fig. 8) suggests a genetic relationship. The discussed mineral assemblage occurs in a characteristic manner. In bioclastic reefs and in porous spaces (porosity, microfractures) it crystallizes in the following order: calcite ± (Fe-dolomite) ± chalcocite ± hematite (akaganeite, lepidocrocite) ± Ag-chloride ± Ag-amalgams ± chevrel compound $(K,Cu)Mo_2(S,Cl)_5$ ± gypsum ± sylvite. The observed order of crystallization generally follows solubility constants in water. Crystallization of 1 cm^3 of gypsum consumes 0.48 g of water, this in micro porous environment is more than enough to locally cause even precipitation of KCl due to oversaturation (Fig. 8; Kucha, Pawlikowski 2010);

(ii) even larger quantity of sylvite appears to be associated with $(K,Cu)Mo_2(S,Cl)_5$ in subhorizontal veins and nests in black shale bottom. Sylvite forms veinlets and euhedral cubes with size of up to 3 mm inside chevrel. The other main minerals are gypsum, carbonates, annabergite, erithrite and Co-Ni di-arsenides. The occurrence of KCl has been confirmed by both XRD and microprobe.

4.4. Au-Ag-Cu solid solution series

The main mineral of gold is Ag-Au solid solution forming grains from sub μ up to 3 mm, most often around a few μm. On the reduced side of the redox interface gold grains are silver rich but on the oxidized side of the interface the Au content may reach exceptionally up to 97.40 wt% in sample from dolomitc reef from the Lubin West Mine (Kucha 1981). The following characteristic microtextures are visible within grains of Au-Ag solid solution from oxidized side of the redox interface:

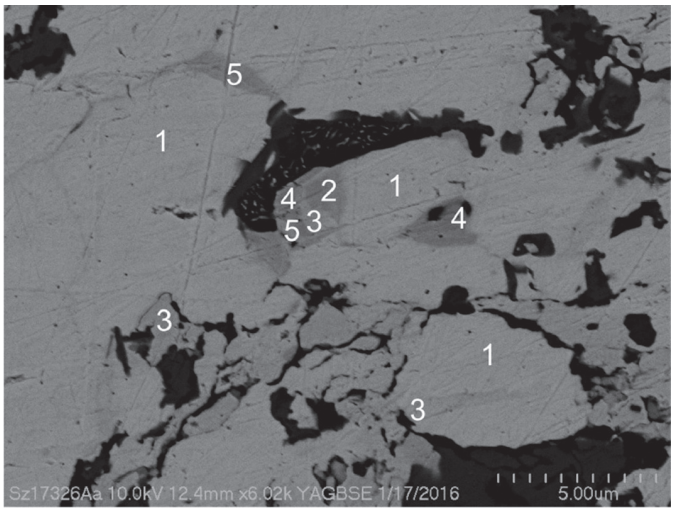

Figure 9. YAGBSE picture of zoned gold from the Sieroszowice Mine redox interface. Brightest gold contains the highest Au content, darker gold contains increasing Ag content (see Table A15 with respective chemical composition of gold). Sample Sz1732/6Aa.

(i) distinctly zoned Au-Ag solid solutions from the Siertoszowice/Polkowice Mine (Fig. 9; Table A15);

(ii) two phase gold, where in the Au rich matrix smaller Ag-rich grains occur at the redox interface at the Lubin West Mine (Kucha, Pochec 1983);

(iii) two phase gold where Au-rich grains occur in Ag-rich matrix (Fig. 5b);

(iv) rarely occurring oscillatory Au-Ag zoning observed at the strongest redox gradient at Polkowice-Sieroszwice Mine (Fig. 5b).

Gold at the oxidized side of the redox interface is rarely accompanied by tetraauricupride (Table A15) first described from Polkowice-Sieroszowwice Mine in 1988 (Piestrzyński, Pieczonka 1998).

4.5. Sperrylite $PtAs_2$, geversite $(Pt,Pd)(Sb,Bi)_2$ and insizwaite $Pt(Bi,Sb)_2$

Platinum and Bi content in the clay organic-matrix of NMBS free of microscopically visible ore mineral inclusions measured by μPIXE is (ppm): ≤ 12.5 - 233.3 (av 108.7; n = 18), and Bi ≤ 9 - 773 (av. 224) (Table A16; based on Kucha et al. 1993, 1994, 1999; Przybyłowicz et al. 1990, 1992; and new measurements). Platinum and Bi content in organic matrix of thucholite free of microscopically visible minerals is (ppm, μPIXE): Pt = 15.2 - 464.9 (av 123.0; n = 48), Bi ≤ 44.8 - 2693, and by SXRFA; Pt ≤ 2 - 1770 (av 162, n = 21) and Bi ≤ 45.8 - 2900 (Table A16). Many trials to find self Pt minerals over the years failed. Microarea study of organic matrix of thucholite by microprobe and TEM indicates correlation Pt-Ni-V suggesting substitution of Pt in tetrapyrrole ring (Kucha 1982; Kucha, Przybyłowicz 1999). Some Pt was also found in Pd arsenides, which are very rare minerals, and therefore cannot explain Pt values detected by μPIXE and SXRFA (Table A16). It was therefore concluded that Pt persistently hides in organic matter.

Progress of research on the Kupferschiefer redox-interfaces indicates that there are several stages of development of redox-interfaces confirmed by Re-Os dating (Alderton et al. 2016) and U-Pb dating (Kucha, Przybyłowicz 1999; Kucha; 2003; Mikulski, Stein 2010, 2015, 2017). These events occurred at different time and brought up a different contingent of metals. U-Pb dating of thucholite nodules with noble metals, calculated from the 'A' component free of visible mineral micro-grains, yields an age of 175 - 180 Ma, and might have been related to the Lower Jurassic extension tectonics (Kucha, Przybyłowicz 1999). The main redox interface, with the strongest redox gradient is present on the western side of the Cu-mining area. Red colored rocks show strong red color coming from dispersed fine hematite ± akaganeite (Fig. 6a). NMBS has a grey color with reddish spots. Copper content is very low and varies between

0.05 to 0.15 wt%, TOC content varies in the range of 0.2 - 0.40 wt%. Platinum content may reach locally a 25 ppm level in a few mm thick NMBS, where Cu sulphides anilite, digenite, yarrowite, spionkopite, covellite and bornite are containing inclusions of gold, geversite, insizwaite, and clausthalite (Fig. 6b). The matrix of red boundary dolomite is composed of (XRD): calcite, dolomite, anhydrite, gypsum, kaolinite 1Md, quartz, and hematite ± akaganeite.

The NMBS has a grey color with reddish spots (Fig. 6a). It contains rare sulphide grains composed of anilite, digenite, yarrowite, spionkopite, clausthalite and covellite (Fig. 6b). Inside Cu-sulphide clots small inclusions with size from a few to 90 µm of two-phase gold (Fig. 5) and a few to 20 µm large inclusions of sperrylite (Fig. 5a) and a few to 10 µm large grains of geversite and insizwaite (Fig. 6b,c) occur. All three minerals are isotropic, and have high reflectivity. They form direct intergrowths and despite similar optical properties can be distinguished because sperrylite has distinctly higher polishing hardness, geversite has R% in air at λ = 550 nm (white light) higher by 5% measured as 59% using synthetic pyrite standard, and insizwaite has much higher average Z number and therefore it appears much brighter on BSE pictures than the two other associated Pt minerals (Fig. 6c).

Sperrylite has relatively small admixture of Sb and Bi (Table A17) and usually contains a few wt% of Pd. Geversite has almost equal amount of mol Sb and mol Bi (Table A17), but it is distinctly brighter (by 5%) in reflected light than intergrown insizwaite. Insizwaite has a high admixture of Sb, but it is easily distinguished from the others because it forms well pronounced euhedral crystals (Fig. 6c).

It is speculated whether these Pt minerals can be recovered or not? In technical terms it is possible either by:

(i) gravity separation because Pt + native gold is present inside Cu sulphide clots (Table A18), but simultaneously the process would pick up associated metazunerite, metauranospinite and uranospinite which may pose thread to the environment;

(ii) flotation would pick up Cu sulphide clots together with gold inclusions and Pt arsenide-antimonide-bismuthides. Unfortunately, the Cu content is so low in this NMBS that it will not pay back the costs of the whole operation.

4.6. Cinnabar HgS

Cinnabar is a very rare mineral in the studied deposit. So far it has been found only in two samples collected at the major redox interface on the western perimeter of the Kupferschiefer mining area together with metazunerite-metauranospinite and uranospinite, Au-Ag ss, teterauricupride, tennantite, sulfo-arsenides of Co, Ni and Cu, di-arsenides of Ni and Co and nickeline, hematite, goethite ± akaganeite, cinnabar (Fig. 4b,c), $PtAs_2$, $Pt(Sb,Bi)_2$ and $PtBi_2$. Euhedral cinnabar is encapsulated in overgrown euhedral quartz, and this probably protected it from latter replacement.

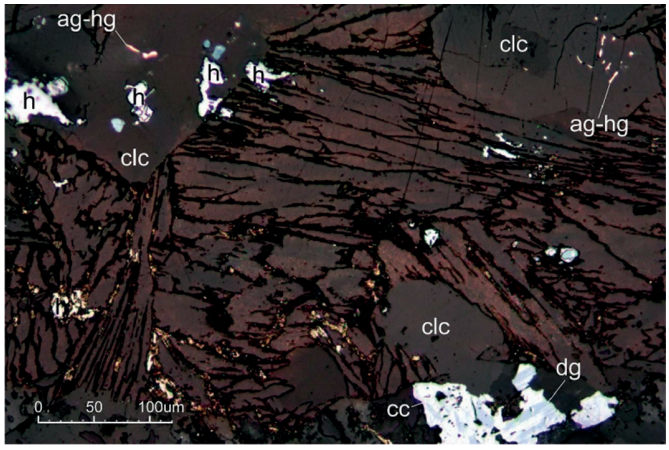

Figure 10. Photomicrograph of sub-horizontal veinlet in the top part of white sandstone filled up by celestine-barite laths reddened by hematite grains (h) and dispersed fine hematite nebular powder. Veinlet is flanked by large calcite grains (clc) containing multiple inclusions of silver amalgams (ag-hg) and chalcocite (cc) and digenite (dg). Reflected light, sample 4_3LZM.

Samples containing cinnabar contain also fine Cu-Hg-selenide-sulphides which are close to the following chemical formulas: $Cu_3(Ag,Au)_1Hg(S,Se)_4$, $(Cu,Ag)_3Hg_3(Se,S)_5$, $Cu_{3.5}Hg_{2.5}(S,Se)_5$, $(Cu,Ag,Au)Hg(Se,S)_3$, $(Cu,Ag,Au)_6Hg(S,Se,Cl)_6$. They have different optical properties in reflected light but need to be studied by TEM diffraction and Raman to define their crystallographic status.

4.7. Celestine-barite solid solution

Celestine-barite solid solution is (Table A19) one of the main accessory minerals in the Kupferschiefer. It occurs as infills of micro-porosity and as distinct veinlets composed from large laths of zoned celestine-barite (Fig. 10). The most common celestine-barite has Sr/Ba ratio around 2.5 and 7.5 (Table A19). Celestine-barite in deeper part of the Kupferschiefer in the Rudna Mine has small relict inclusions of barite. Celestine-barite forms distinct laths with size up to 350 µm in length. They are zoned with the central part of laths usually containing more Ba than Sr. Calcite flanking the discussed sub horizontal veinlets contains ubiquitous inclusions of Ag-amalgams kuestelite, eugenite and schachnerite. Euhedral uraninite grains associated with celestine-barite give U/Pb age of 84 ± 1 Ma, based on four measurements of euhedral UO_2 grains.

5. Final remarks

An average concentration of U in Cu black shale in the Lubin and Polkowice mines is 166.5 ppm (Piestrzyński

1990) and in thucholite shale is 180 ppm. The P_2O_5 concentration in typical Cu black shale varies from 0.07 to 0.16 wt% (KGHM channel samples), in Zn-bearing shale 0.09 - 0.88 wt%, in the NMBS 0.31 - 1.60 wt% but this shale is only 5 mm thick. In the NMBS white phosphate lenses are intergrown with β-boracite (Kucha 1982, 1983). The P_2O_5 content may reach locally 1.0 - 1.5 wt% in biogenic limestone with native alloys of Au-Ag, Pt, Pd and Pb-Au, with phosphates and red stains of β-hydrohematite (Kucha 1981). Bioclastic limestone (bioclastic reefs partly dolomitized) occur instead of black shale and has features indicating hard ground processes (Kucha, Pochec 1983).

To compare average P content in black shale against metal contents within phosphates we need to dilute contents in phosphates roughly by ~200 times. Such a comparison suggests that amount of Ca phospates in the shale cannot explain too well observed average REE values in the shales (Table A20). Therefore integrated observations suggest that REE and U are controlled by brannerite, monazite-huttonite and florencite in the mineralized Kupferschiefer (Tables A7, A8, A9, A20). Such an observation agrees well with circulation of the mineralizing fluids within fractured basement (Blundell et al. 2003) coupled with several repetitions of the process delivering different sets of elements and upgrading the ore (Alderton et al. 2016). Occurrence of florencite mainly within Mo-Re-shales together with celestine and hematite my support notion that hematitic cements within Rotliegedes (Michalik 2001) were also a source of metals for the Kupferschiefer mineralization.

Acknowledgements

I would like to thank M. Michalik for help to produce informative but very laborious scanning pictures of noble metals, chlorides and U minerals presented in this paper. S. Mikulski and two anonymous reviewers are acknowledged for their comments. I. Klonowska is thanked for the final preparation of the manuscript.

References

Alderton, D.H.M., Selby, D., Kucha, H., & Blundell, D.J. (2016). A multistage origin for Kupferschiefer mineralization. *Ore Geology Reviews, 79,* 535-543. DOI: 10.1016/j.oregeorev.2016.05.007

Banaś, M., Jarosz, J., & Salamon, W. (1978). Thucholite from the Permian Cooper- bearing rocks in Poland. *Mineralogia Polonica, 9,* 3-22.

Blundell, D.J., Karnkowski, P.H., Alderton, D.H.M., Oszczepalski, S., & Kucha, H. (2003). Copper mineralization of the Polish Kupferschiefer: A proposed basement fault-fracture system of fluid flow. *Economic Geology, 98,* 1487-1495. DOI: 10.2113/gsecongeo.98.7.1487

Burns, P. C., & Li, Y. (2002). The structures of becquerelite and Sr-exchanged becquerelite. *American Mineralogist, 87,* 550-557. DOI: doi.org/10.2138/am-2002-0418

Kucha, H. (1974). Native gold in the copper deposits from the Fore-Sudetic Monocline. *Rudy Metale, 4,* 174-175 [in Polish].

Kucha, H. (1975). Preliminary report on the occurrence of palladium minerals in the Zechstein rocks of the Fore-Sudetic Monocline. *Mineralogia Polonica, 6,* 87-93.

Kucha, H. (1976). Platinum, palladium, mercury and gold in the Zechstein rocks of the Fore-Sudetic Monocline. *Rudy Metale, 1,* 24-25 [in Polish].

Kucha, H. (1990). Geochemistry of Kupferschiefer, Poland. *Geologische Rundschau, 79,* 387-399.

Kucha, H. (2003). Geology, mineralogy and geochemistry of Kupferschiefer, Poland. In J.G. Kelly, C.J. Andrew, J.H. Ashton, M.B., Boland, E. Earls, L. Fusciardi, & G. Stanley (Eds), *Europe's Major Base Metal Deposits* (pp. 215-238). Dublin: Irish Association for Economic Geology.

Kucha, H., & Wieczorek, A. (1980). $Ca_{1-x}Th_{1-x}RE_{2x}(PO_4)_2 \cdot 2H_2O$, a new mineral from Lower Silesia, Poland. *Mineralogia Polonica, 11,* 123-132.

Kucha, H. (1981). Precious metal alloys and organic matter in the Zechstein copper deposits, Poland. *Tschermaks mineralogische und petrographische Mitteilungen, 28,* 1-16.

Kucha, H. (1982). Platinum metals in the Zechstein copper deposits, Poland. *Economic Geology, 77,* 1578-1591.

Kucha, H. (1983). Precious metal bearing shale from Zechstein copper deposits, Lower Silesia, Poland. Transactions of the Institution of Mining and Metallurgy. Section B. *Applied Earth Science, 92,* 72- 79.

Kucha, H., & Głuszek, A. (1983). Variation of Cu-Zn-Pb-Ag mineralization in the deposit of the Lubin Mine. *Annales Societatis Geologorum Poloniae, 53,* 143-168.

Kucha, H. (1984). Palladium minerals in the Zechstein copper deposits in Poland. *Chemie der Erde, 43,* 27-43.

Kucha, H. (1993). Noble metals associated with organic matter, Kupferschiefer, Poland. In J. Parnell, H. Kucha, & P. Landais (Eds), *Bitumens in ore deposits* (pp. 153-170). Springer: SGA Special Publications.

Kucha, H. & Przybyłowicz, W. (1999). Noble metals in Organic Matter and Clay- Organic Matrices, Kupferschiefer, Poland. *Economic Geology, 94,* 1137-1162. DOI: doi.org/10.2113/gsecongeo.94.7.1137

Kucha, H., & Pochec, J. (1983). Organogenic ankeritic limestone with glauconite and native Au, Pt, Pd and Pb alloys in the region of Lubin (Western Poland). *Annales Societatis Geologorum Poloniae, 53,* 169-176.

Kucha, H., Przybyłowicz, W., Lankosz, M., Langevelde van, F., & Traxel, K. (1993). EPMA, micro-PIXE, synchrotron microprobe and TEM study of visible and invisible accumulations of Au and PGE in black shale and organic matrix, Kupferschiefer, Poland. *Mineralogical Magazine, 57,* 103-112. DOI: 10.1180/minmag.1993.057.386.10

Kucha, H., & Pawlikowski, M. (2010). Genetic investigations of copper Zechstein deposits, Poland. *Geologia, 36*(4), 513-538 [in Polish].

Michalik, M. (2001). Diagenesis of the Wessliegend sandstones in the south-western margin of the Polish Rotlegend Basin. *Prace Mineralogiczne, 91,* 1-176.

Mikulski, S.Z., & Stein, H.J. (2010). Re-Os age of a chalcopyrite sample from the Lubin Cu-Ag mine, Kupferschiefer, SW Poland. *Geochimica et Cosmochimica Acta*, *71*(07S):A708, Suppl. S.

Mikulski, S.Z., & Stein, H.J. (2015). Re-Os ages for Ag-bearing Cu sulphide ores from the Kupferschiefer in Poland. Proceeding of the 13th Biennial SGA Meeting, 24-27 August 2015 (pp. 607-610). Nancy, France, Université de Lorraine.

Mikulski, S.Z., & Stein, H.J. (2017). Wiek izotopowy Re-Os siarczkowej mineralizacji Cu-Ag oraz jej charakterystyka mineralogiczna i geochemiczna - obszar złożowy Lubin - Polkowice (SW Polska). *Biuletyn Państwowego Instytutu Geologicznego, 468,* 79-96. DOI:10.5604/01.3001.0010.0105.

Oszczepalski, S., Chmielewski, A., & Mikulski, Z. (2016). Controls on the distribution of rare earth elements in the Kupferschiefer series of SW Poland. *Geological Quarterly, 60*(4), 811-826.

Pagoaga, M.K., Appleman, D.E., & Stewart, J.M. (1987). Crystal structures and crystal chemistry of the uranyl oxide hydrate becquerelite, billietite, and protasite. *American Mineralogist, 72*, 1230-1238.

Piestrzyński, A. (1990). Uranium and thorium in the Kupferschiefer formation, Lower Zechstein, Poland. *Mineralium Deposita, 25,* 146-151.

Piestrzyński, A. & Pieczonka, J. (1998). Tetraauricupride from the Kupferschiefer type deposit, SW Poland - first occurrence. *Mineralogia Polonica, 29,* 11-18.

Piret-Meunier, J. & Piret, P. (1982). Nouvelle determination de la structure cristalline de la becquerelite. *Bulletin de Mineralogie, 105*(6), 606-610.

Przybyłowicz, W., Kucha, H., Kajfosz, S., & Szymczyk, S. (1990). PIXE analysis of Kupferschiefer samples. In S. Jasieńska, & L.J. Maksymowicz (Eds), *Academy of Mining & Metallurgy* (pp. 928). Cracow: 12th International. Congress on X-ray Optics & Microanalysis.

Przybyłowicz, W., Langevelde van, F., Kucha, H., Lankosz, M., & Wyszomirski, P. (1992). Trace element determinations in selected geological samples using a 15 keV synchrotron microprobe at the SRS, Daresbury, UK. *Nuclear Instruments and Methods in Physics Research, B68,* 115-121.

Rydzewski, A. (1978). Facja utleniona cechsztyńskiego łupku miedzionośnego na obszarze monokliny przedsudeckiej. *Przegląd Geologiczny, 26*(2), 102-108.

Salamon, W., & Banaś, M. (2002). Coffinite from the Permian copper-bearing ores, SW Poland. *Mineralogia Polonica, 33*(1), 3-16.

Supplementary files

Supplementary data associated with this article (Tables A1–A20) can be found in the online version, at https://doi.org/10.2478/mipo-2021-0004.

Received: 10 July 2017
Accepted: 04 February 2022
Handling Editors: Marek Michalik, Jarosław Majka